Proceedings of the 2025 SICE Festival with Annual Conference
September 9-12, 2025, Chiang Mai, Thailand

Non-contact generation of converging ultrasound based on sub-terahertz photoacoustic effect at air-water spherical boundaries

Yuki Morimoto[1], Tatsuma Kawanishi[2], Masahiko Inami[3], and Yasuaki Monnai[4]

[1]Department of Medical Engineering, Faculty of Engineering, Chiba University, Chiba, Japan
(E-mail: ymorimoto-tky@umin.ac.jp)
[2]Department of Mathematical Engineering and Information Physics, Faculty of Engineering, The University of Tokyo, Tokyo, Japan
(E-mail: kawanishi@g.ecc.u-tokyo.ac.jp)
[3]Research Center for Advanced Science and Technology, The University of Tokyo, Tokyo, Japan
(E-mail: drinami@star.rcast.u-tokyo.ac.jp)
[4]Research Center for Advanced Science and Technology, The University of Tokyo, Tokyo, Japan
(E-mail: monnai@star.rcast.u-tokyo.ac.jp)

Abstract: The terahertz photoacoustic effect enables non-contact generation of plane-wave ultrasound in aqueous media. However, for applications such as biomedical imaging, wavefront engineering is crucial for enhancing spatial resolution and signal-to-noise ratio. In this study, we explore the feasibility of non-contact implementation of ultrasound wavefront engineering through a geometric approach. We demonstrate that sub-terahertz waves impinging onto a spherical water boundary formed within an acrylic spherical tank can generate focused ultrasound in water owing to the geometric effect. We experimentally observe a focused wavefront by translating a hydrophone. This capability of non-contact generation of focused ultrasound has significant potential for sensing and imaging.

Keywords: Terahertz wave, Photoacoustic effect, Ultrasonic convergence, Wavefront engineering, Biomedical imaging

1. INTRODUCTION

The photoacoustic effect is a phenomenon in which electromagnetic irradiation causes the thermal expansion of a medium, resulting in the generation of acoustic signals [1], [2]. Based on this effect, photoacoustic imaging has been actively investigated for clinical applications over the past two decades [3]. Pushed by the progress of high-power visible light laser technologies, conventional photoacoustic biomedical imaging has evolved and been applied in clinical areas such as breast imaging, dermatologic imaging, and vascular imaging [4], [5]. These applications capitalize mainly on the absorption of visible light by chromophores in human tissue, such as hemoglobin, melanin, and lipids [6].

Recent terahertz (THz) technology advancements have enabled tabletop-scale THz wave sources and beam steering systems [7]. This opens new possibilities for THz-based photoacoustic biomedical imaging [8]. THz waves exhibit significantly stronger absorption in water than visible light, while not reaching that of mid-infrared light [9]. In the absence of an adequate mid-infrared laser light source, applying terahertz waves in biomedical measurements enables substantially unique approaches [10]. When a THz wave is irradiated onto an aqueous medium, efficient energy transfer from the THz wave to thermal energy occurs, causing a thin layer near the medium boundary to serve as the source of acoustic signals [11]. It has been demonstrated that modulated continuous-wave sub-THz waves can efficiently generate ultrasound signals when irradiated from air into water [12]. The generation of in-vivo ultrasound in a non-contact manner has also been demonstrated [8].

To achieve non-contact biomedical imaging based on ultrasound induced by THz waves, it is crucial to develop wavefront engineering, including beam focusing, for enhancing spatial resolution and signal-to-noise ratio. The well-known versatile technique for ultrasound wavefront engineering is the phased array, which consists of individually phase-controlled radiation elements and is commonly used in ultrasound imaging. However, the use of ultrasound phased arrays necessitates conventional contact-type transducers. While a previous study by Hirata et al.[12] has investigated the photoacoustic effect at a planar air-water boundary, where the irradiated surface of the aqueous medium forms a uniform acoustic source, the effects of non-planar boundary geometries could involve an effect analogous to acoustic lenses. Based on this concept, we explore the feasibility of wavefront engineering through geometric modifications of the medium surface. We experimentally verify the convergence of ultrasound induced by the sub-THz photoacoustic effect through the proposed approach.

2. METHOD

2.1 Concept

The concept of the proposed method is illustrated in Fig. 1. It has been demonstrated that when a THz wave is

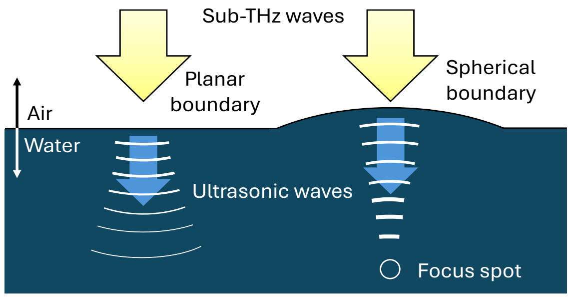

Fig. 1 Conceptual illustration comparing ultrasound propagations based on the photoacoustic effect at a planar and spherical boundary.

irradiated onto a planar boundary, each point on the irradiated surface acts as a secondary wave source, defining a uniform radiation aperture. The elementary waves generated from this aperture propagate through the water as a collimated beam, which begins to spread after the Rayleigh distance [13]. In contrast, here we utilize a spherical boundary to position the secondary wave sources along the curved surface. As a result, the elementary waves originating from these sources are expected to propagate in a way that constructively interfere toward the center of the sphere, where the path lengths become equal. In other words, the spherical boundary not only facilitates the photoacoustic effect but is also expected to function as a lens that converts the incident THz plane wave into a converging ultrasound.

2.2 Theory

The wave behavior generated by the photoacoustic effect can be analyzed using Huygens' principle. Kirchhoff mathematically substantiated this principle, leading to the following approximations [14].

1. Fresnel Approximation

When the distance r from the antenna aperture is significantly larger than the wavelength λ, the distribution of the complex amplitude of the wave, A, can be expressed using the following equation.

$$A(x,y,z) = \frac{1}{j\lambda}\iint_{\Sigma} A(\xi,\eta,0)\frac{\exp(-jkr)(1+\cos\varphi)}{2r}d\xi d\eta \quad (1)$$

Here, ξ and η represent the coordinates in the x and y directions on the aperture plane, while k and φ denote the wavenumber and phase components of the wave, respectively.

2. Fraunhofer Approximation

A further approximation can be applied for cases involving infinitely distant observation points or focal planes formed by a lens. In such cases, the amplitude distribution is given by the following equation, which corresponds to a two-dimensional Fourier transform.

$$A(x,y,z) = \frac{\exp(-jkz)}{jz\lambda}\iint_{\Sigma} A(\xi,\eta,0)\exp\left(jk\left[\frac{x\xi}{z}+\frac{y\eta}{z}\right]\right)d\xi d\eta \quad (2)$$

Thus, based on the assumption of the lens effect, the ultrasound amplitude distribution at the center of a spherical boundary can be analyzed using the Fraunhofer approximation.

2.3 Experimental Construction

In this study, we use water tanks of two different shapes to investigate the behavior at the spherical water-air boundary. The experimental system is constructed as follows (Fig. 2 (a) and (b)). First, a 15.43 GHz microwave is generated using an oscillator. The microwave is multiplied six times by an amplifier-multiplier chain, producing a 92.6 GHz sub-THz wave. The sub-THz wave is modulated at 1.1 MHz using a PIN diode modulator with a function generator. The modulated sub-THz wave is then amplified by a GaN power amplifier. We estimate the amplified power to be 0.65 W.

The sub-THz wave is then radiated via a horn antenna with a rectangular aperture of 21 mm × 30 mm and is perpendicularly irradiated onto a side of the water tank.

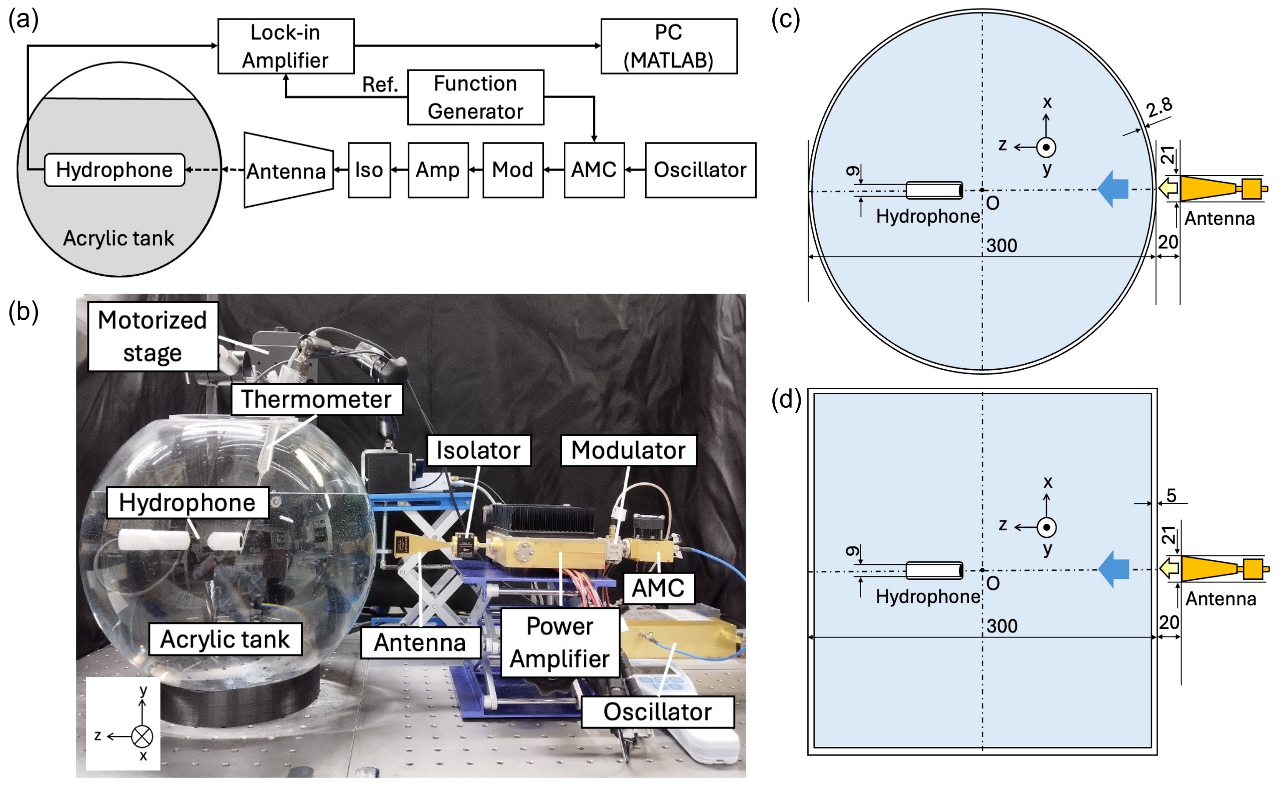

Fig. 2 Schematic (a) and photograph (b) of the experimental setup for photoacoustic signal generation by sub-THz irradiation and detection with a hydrophone. (c, d) The geometry of the horn antenna, water tanks, and hydrophone. Panel (c) shows the setup for a spherical boundary, while panel (d) shows the setup for a planar boundary.

The spherical water tank is made of acrylic, with a diameter of 30 cm and a wall thickness of 2.8 mm. The rectangular water tank is also acrylic with a side length of 30 cm and a thickness of 5 mm. Each tank is positioned so that the sub-terahertz wave is irradiated perpendicularly onto the surface along the Z-axis, directed toward the center of the tank. The water level inside the tanks is at a height of 40 mm above the center of the irradiation area. The geometric details of each configuration are shown in Fig. 2 (c) and (d). We place a hydrophone with a sensitivity of 6.3 μV/Pa inside the water tank with its sensing surface oriented toward the sub-terahertz wave irradiation area. The hydrophone signal is amplified by 40 dB with a preamplifier and connected to a lock-in amplifier. The position of the hydrophone is controlled with a three-axis motorized stage. The lock-in amplifier is synchronized with the function generator modulating the sub-terahertz wave. All devices are connected to a laptop and controlled via MATLAB.

The ultrasound was scanned with the hydrophone according to the following protocol. The origin is set at the center of each water tank, which is visually aligned. Each measurement is performed with a time constant of 1 second, with a 5-second stabilization period between measurements. The water temperature during the experiment is maintained between 19.5°C and 23.0°C. The experiment is conducted in the following sequence: measurements are first taken in the spherical water tank, starting with the signal measurement, followed by the noise measurement, and then in the rectangular water tank with the same procedure.

3. RESULTS & DISCUSSION

3.1 Results

The heatmap of the ultrasound distribution in the XZ plane acquired by the hydrophone for the spherical and planar boundary is shown in Fig. 3 (a) and (b), respectively. A single beam propagating in the Z-direction, centered at X=0, is observed in each case. Both beam widths remain nearly constant, exhibiting collimated beams. The beam width generated with the spherical boundary is narrower compared to that with the planar boundary. Periodic fringes are observed along the Z-axis in both cases. These fringes are presumed to be caused by multiple reflections, i.e., standing waves, between the water tank walls and the plane of the hydrophone sensing surface. Figures 3 (c) and (d) show the cross-sectional profiles along the X-direction at Z=0. The beam width, defined by the full width at half maximum (FWHM) of the acoustic intensity, is 6.0 mm for the spherical boundary, whereas it is 14.5 mm for the planar boundary, demonstrating the focusing effect of the spherical geometry.

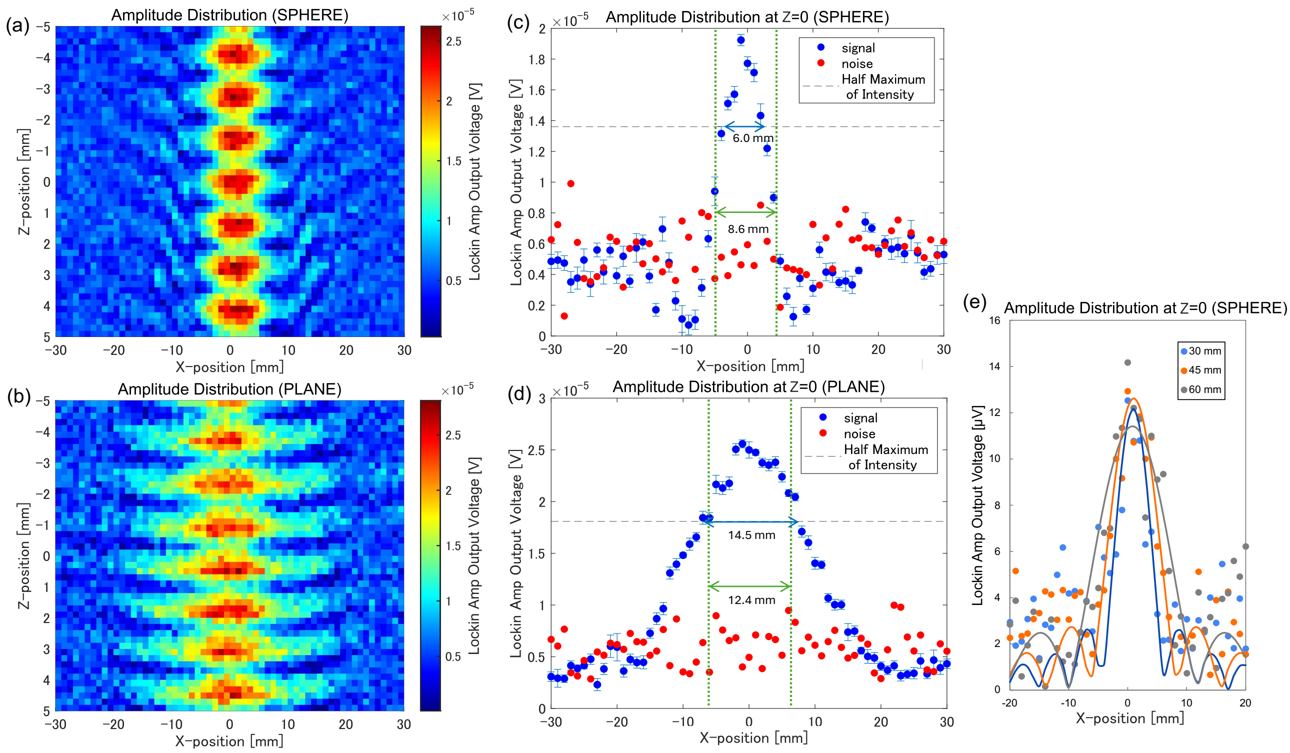

Fig. 3 Heatmap of amplitude distribution in signal measurement for spherical boundary (a) and planar boundary (b). Amplitude distribution along the X-direction at Z=0 for spherical boundary (c) and planar boundary (d). Black horizontal dashed lines indicate the half-maximum intensity level, and green vertical dashed lines denote the theoretical half-width for each condition. Signal measurements were repeated five times at each point; plots show the mean value, with error bars representing the standard deviation. (e) Amplitude distribution measured at Z=0 for varying water levels, using a spherical boundary. Experimental values are shown for three levels: 30 mm (blue), 45 mm (orange), and 60 mm (gray). The solid curves are fitted *sinc* functions corresponding to each dataset.

3.2 Discussion

The theoretical amplitude distribution of the ultrasound at the origin for the spherical boundary is calculated using a Fraunhofer approximation for a rectangular aperture. With the aperture width in the X-direction as $2a$, the amplitude distribution at Y=0, Z=0 is given by a *sinc* function as follows.

$$A(x) = \sin\left(\frac{ka}{R}x\right)/\frac{ka}{R}x \quad (3)$$

Substituting an aperture width of $2a = 21$mm, angular wavenumber $k = 2\pi/\lambda = 10.36$ rad/mm, and focal distance $R = 150$ mm, the numerical calculation of the FWHM of the intensity results in a theoretical beam width of 8.6 mm.

In the case of a planar boundary, as long as the observation point lies within the Rayleigh distance, the beam width remains nearly constant during propagation. In this experiment setup, the THz irradiation region can be approximated as a circular aperture of radius a, yielding a Rayleigh distance of 254 mm $(= \pi a^2/\lambda)$. Since the origin is located at $R = 150$ mm—well within the Rayleigh distance—the beam is expected to maintain its initial width. Assuming a Gaussian beam profile, the FWHM of the intensity distribution at the origin is estimated to be approximately 12.4 mm.

In the experiment, the beam width for the spherical boundary is slightly narrower than the theoretical value. This discrepancy is considered to be due to interference with reflected sound waves from the water surface above. As an additional experiment, the water level at the Y-coordinate is varied to 30, 45, and 60 mm using the spherical water tank. As shown in Fig. 3 (e), changes in the beam width are observed. We thus demonstrated that ultrasound converging was influenced by the reflection at the water surface above. Further investigation is necessary to quantitatively evaluate the effect of reflected waves, as similar interferences are expected to occur in biomedical measurement subjects.

4. CONCLUSION

We investigated the effects of a geometric approach to the air-water boundary in non-contact ultrasound generation using the sub-terahertz photoacoustic effect. By shaping the boundary with different water tank designs, we demonstrated that convergent ultrasound generation is achievable with spherical geometry. This simple approach can significantly contribute to spatial resolution and signal-to-noise ratio, opening up new possibilities for non-contact ultrasound biomedical imaging.

ACKNOWLEDGMENTS

This work was supported by JSPS KAKENHI 24H00704.

REFERENCES

[1] A. G. Bell, "THE PRODUCTION OF SOUND BY RADIANT ENERGY," *Science (1979)*, vol. os-2, no. 49, pp. 242–253, May 1881, doi: 10.1126/science.os-2.49.242.

[2] V. E. Gusev and A. A. Karabutov, "Laser Optoacoustics."

[3] J. J. M. Riksen, A. V. Nikolaev, and G. van Soest, "Photoacoustic imaging on its way toward clinical utility: a tutorial review focusing on practical application in medicine," *J Biomed Opt*, vol. 28, no. 12, Jun. 2023, doi: 10.1117/1.jbo.28.12.121205.

[4] P. K. Upputuri and M. Pramanik, "Recent advances toward preclinical and clinical translation of photoacoustic tomography: a review," *J Biomed Opt*, vol. 22, no. 4, p. 041006, Nov. 2016, doi: 10.1117/1.jbo.22.4.041006.

[5] A. B. E. Attia *et al.*, "A review of clinical photoacoustic imaging: Current and future trends," Dec. 01, 2019, *Elsevier GmbH*. doi: 10.1016/j.pacs.2019.100144.

[6] A. Taruttis and V. Ntziachristos, "Advances in real-time multispectral optoacoustic imaging and its applications," *Nat Photonics*, vol. 9, no. 4, pp. 219–227, Mar. 2015, doi: 10.1038/nphoton.2015.29.

[7] Y. Monnai, X. Lu, and K. Sengupta, "Terahertz Beam Steering: from Fundamentals to Applications," Apr. 01, 2023, *Springer*. doi: 10.1007/s10762-022-00902-1.

[8] N. Ichikawa and Y. Monnai, "Generating in vivo continuous ultrasound based on sub-terahertz photoacoustic effect," *APL Photonics*, vol. 8, no. 8, Aug. 2023, doi: 10.1063/5.0157652.

[9] H. D. Downing and D. Williams, "Optical constants of water in the infrared," *J Geophys Res*, vol. 80, no. 12, pp. 1656–1661, Apr. 1975, doi: 10.1029/JC080i012p01656.

[10] J. Li *et al.*, "Time-domain terahertz optoacoustics: Manipulable water sensing and dampening," *Advanced Photonics*, vol. 3, no. 2, Mar. 2021, doi: 10.1117/1.AP.3.2.026003.

[11] M. Tsubouchi, H. Hoshina, M. Nagai, and G. Isoyama, "Plane photoacoustic wave generation in liquid water using irradiation of terahertz pulses," *Sci Rep*, vol. 10, no. 1, Dec. 2020, doi: 10.1038/s41598-020-75337-6.

[12] T. Hirata, M. Inami, and Y. Monnai, "Sub-terahertz photoacoustic effect enabling broadband ultrasound generation for underwater communication," *APL Photonics*, vol. 8, no. 9, Sep. 2023, doi: 10.1063/5.0160360.

[13] J.-Y. Lu, H. Zou, and J. F. Greenleaf, "Biomedical ultrasound beam forming," *Ultrasound Med Biol*, vol. 20, no. 5, pp. 403–428, Jan. 1994, doi: 10.1016/0301-5629(94)90097-3.

[14] D. Headland, Y. Monnai, D. Abbott, C. Fumeaux, and W. Withayachumnankul, "Tutorial: Terahertz beamforming, from concepts to realizations," May 01, 2018, *AIP Publishing*. doi: 10.1063/1.5011063.